Highlights

Condition monitoring of mooring systems for Floating Offshore Wind Turbines using Convolutional Neural Network framework coupled with Autoregressive coefficients

Smriti Sharma,Vincenzo Nava

- Developed a condition monitoring of floating offshore wind turbine mooring system accounting wave randomness and metocean conditions.

- Convolutional Neural Network coupled with Auto-regressive coefficients is proposed for damage identification.

- Auto-regressive model-based data enrichment ensures CNN has feature-enriched data for better performance.

- Performance is compared against alternate machine learning classifiers.

Condition monitoring of mooring systems for Floating Offshore Wind Turbines using Convolutional Neural Network framework coupled with Autoregressive coefficients[★]

Smriti Sharma[a,∗], Vincenzo Nava[a,b]

[a]*Basque Center for Applied Mathematics, Alameda de Mazarredo, 14, Bilbao, 48009, Spain*
[b]*TECNALIA, Basque Research and Technology Alliance (BRTA), Bilbao, Spain*

ARTICLE INFO

Keywords:
Structural health monitoring
Offshore Structures
Damage diagnosis
Wind Turbines
Mooring lines
Auto Regressive Model (AR)
Convolutional Neural Network (CNN)

ABSTRACT

This research presents a novel approach proposed for the monitoring of mooring systems in Floating Offshore Wind Turbines (FOWTs), employing a combination of Convolutional Neural Networks (CNNs) and Auto-Regressive (AR) models. CNN finds broad application in monitoring intricate structures, as they adeptly handle noisy response data without necessitating profound domain expertise. The precision of CNNs relies on the extraction of meaningful features from input data, necessitating meticulous data curation and labeling for optimal computational efficiency and accurate estimation. Emphasis is placed on the preference for feature-rich small datasets over voluminous yet sparse datasets, aiming to enable CNNs to discern crucial patterns more effectively and mitigate issues such as overfitting and extensive preprocessing.

The novelty of the proposed approach lies in the integration of AR models, which serve to compress data and enhance damage-sensitive characteristics in the input for CNNs. This integration involves deploying regression models fitted to historical responses, parameterized with AR coefficients sensitive to damage, and further classifying severity using CNNs. The sequential nature of this approach addresses challenges such as vanishing/exploding gradients, particularly for extended historical data, while also attenuating the impact of noise and irrelevant information through data compression.

The study explores the effectiveness of the coupled AR-CNN method in monitoring FOWT mooring lines, with a specific focus on two levels of damage identification: detection with classification and damage severity across diverse damage and operational scenarios. The modified methodology exhibits superior outcomes by conducting a performance analysis against traditional CNNs and other machine-learning methods, highlighting the potential of the AR-CNN strategy to improve the precision of FOWT mooring line condition monitoring. These findings underscore the AR-CNN strategy's potential to enhance the accuracy of FOWT mooring line condition monitoring.

1. Introduction

Research on the performance and sustainability of FOWTs has made significant strides, supported by the surge of these technologies in related industries. Maintaining these structures within safety and serviceability limits while ensuring optimal maintenance costs has been a major concern for decades. In the context of industrial applications, structural health monitoring (SHM) techniques, especially when approached using data-driven methodologies, have been appreciated for their noise robustness and cost-effectiveness concerning the benefits earned (Tygesen et al., 2018) for various structural and mechanical inverse estimation problems. These techniques hinge on the notion of deducing material properties from indirect measurements, bypassing the need for explicit knowledge of system physics. Traditional inverse problems are inherently ill-posed, complicating decision-making by linking measurements to various potential causes. Machine Learning (ML)-based approaches mitigate these challenges by utilizing extensive

∗Corresponding author
✉ ssharma@bcamath.org (S. Sharma)
ORCID(s): 0000-0001-7340-6982 (S. Sharma)

data from real structural systems, leading to superior reliability and predictability for a very wide band of application areas.

The recent surge in the application of such algorithms for damage detection in civil infrastructure (Sharma and Sen, 2021, 2020), onshore wind structures (Schlechtingen and Santos, 2011), or several other applications in different fields of studies corroborate the same. Nonetheless, in the context of research on fault detection in offshore wind structures, such inverse solutions are yet to achieve the desired maturity. This is because the pertinent industry is still in its infancy and consequently, the available data sets are limited. Fortunately, a conceptual framework for such data-driven approaches for general structures (Sharma and Sen, 2023) and especially for the operation of wind farms (Augustyn et al., 2019) has recently been successfully implemented using the concept of a digital twin (instead of the real structure), targeting improvement in future design and increasing the reliability of offshore wind platforms.

With an ML-based system identification framework, typical strategies involve extracting specific damage-sensitive features (DSFs) in either a supervised or unsupervised learning framework. In the unsupervised approach, novelty detection has been prevalent, associating novelty in predefined DSFs with plausible damage scenarios. Statistical methods are subsequently employed to leverage information stored in the novelty index (Yao and Pakzad, 2012; Roy and Das, 2015). While unsupervised approaches have excelled at damage detection, they have struggled with damage localization and quantification. Conversely, supervised techniques, while having the potential to transcend mere detection (Cross et al., 2013), necessitate a substantial dataset of input-output data, either sampled from the system or simulated through a surrogate support model. Nevertheless, given the increasing availability of data for many structure types, supervised algorithms have garnered increasing popularity.

Depending on the employed network architecture, supervised algorithms can function as classifiers or regressors. Their effectiveness is contingent on extensive training using machine learning algorithms like random forest, support vector machine (SVM), multi-layer perceptron (MLP), and others. In the context of detecting damage in structural systems, a crucial challenge is selecting suitable DSFs from response data that accurately represent the investigated damage scenarios. This study emphasizes this aspect concerning the condition monitoring of FOWTs, especially for a sub-component of it, i.e. mooring lines.

1.1. Condition monitoring of mooring lines

Being an essential subsystem for the overall integrity of any FOWT, the importance of monitoring the mooring line has increased significantly in recent years (WindEurope, 2021, 2022). This helped in optimizing the design of support structures, ensuring their economic feasibility (Coulling et al., 2013; Duan et al., 2016). Since damage to the mooring line can substantially impact the stability of the entire system, monitoring its health has remained a concern (Bae et al., 2017). With the use of deep learning (DL) algorithms, researchers can now detect damages in wind system components with greater accuracy (Li et al., 2019; Rafiee et al., 2007). There have been several studies to understand the dynamics of aero-hydro-elastic-mooring coupled systems under extreme wind and wave loading (Li et al., 2019; Liu et al., 2017; Benassai et al., 2014). It is also essential to understand different damage-causing aspects and their impact on mooring line damage, including fatigue degradation (Ma et al., 2013), fatigue damage (Thies et al., 2014), strength capacity (Brindley and Comley, 2014), tension and durability (Banfield et al., 2005), environmental loads (Huang and Pan, 2010), etc. There exist model-based or fuzzy logic-based approaches discussing diagnosis methods for mooring damage (Mentes and Helvacioglu, 2011; Jahangiri et al., 2016; Jamalkia et al., 2016), yet insignificant research on data-driven ML/DL-based approaches has been investigated.

Detecting anomalies within intricate structures like FOWT has found an efficient and cost-effective solution in vibration measurements, offering valuable damage-related insights. In practice, structural damage deteriorates stiffness, imprinting its signature on dynamic responses such as acceleration or displacement. Vibration-based damage diagnosis has proven effective across various domains, including civil, mechanical, aeronautical, naval, and offshore structures (Hoell and Omenzetter, 2016; Nair et al., 2006; Kiremidjian et al., 2011). These approaches utilize both model-dependent and independent techniques to scrutinize operational and structural responses, aiming to pinpoint and isolate anomalies.

In a model-based strategy, the incorporation of a conceptual predictive model becomes crucial. This supplementary model is generally expected to accurately represent system dynamics, yet this can be a challenge for intricate and poorly understood structures like FOWT. In contrast, ML offers distinctive advantages compared to conventional model-based diagnostic methods. ML provides a pathway for unbiased, noise-resistant, and model-independent estimations. Such attributes hold significant promise for health assessment in complex systems, including FOWTs. This opens up avenues to explore ML-based algorithms for intricate FOWT subsystems. An illustrative example of this concept is evident in

the work of (Gorostidi et al., 2023), where an auto-encoder and a basic fully connected deep neural network effectively identify the potential for identifying bio-fouling failure and anchorage displacement in mooring systems by leveraging displacement and rotation data.

1.2. CNN-based SHM for mooring

CNN have proven successful in evaluating structural conditions through image processing, as demonstrated by several researchers (Modarres et al., 2018; Cha et al., 2017; Sharma and Sen, 2020; Tong et al., 2017). In their work, Cha et al. (2017) effectively utilized CNNs to distinguish concrete cracks through images. This comparative analysis also explores the impact of varying shooting distances and external light intensities on recognition outcomes. Another study by Tong et al. (2017) developed three distinct CNN architectures for crack identification, localization, and length estimation in asphalt pavement. Soukup and Huber-Mörk (2014) employed CNNs to detect defects on metal surfaces, improving model performance through regularization techniques. In the realm of corrosion detection, Atha and Jahanshahi (2018) applied CNNs to replace manual inspection practices. Additionally, Xu et al. (2019) introduced an adapted Faster Region-based CNN capable of efficiently pinpointing seismic damage nuances such as spalling, concrete cracking, buckling, and steel exposure. Chen and Jahanshahi (2017) combined CNNs and Naive Bayesian data fusion to identify micro-cracks within noisy environments.

However, the majority of these studies primarily rely on the image processing approach, which becomes complex for monitoring FOWT moorings. Sampling images for such structures is not only intricate but, at times, impractical or even impossible. In light of this challenge, an alternative approach that utilizes arrays of vibration response signals disguised as 1D/2D/3D images has been proposed to leverage the exceptional classification potential of CNNs (Sharma and Sen, 2020). Inspired by the success of CNNs in identifying damage signatures from noisy structural responses, the current study adopts this approach while circumventing the associated challenges of selecting appropriate damage-sensitive features, as elaborated later.

Finally, as previously discussed in this article regarding data-driven estimation methods, the quality of the data remains crucial for achieving accuracy and reliability. Particularly in the context of health assessment, highlighting the presence of damage-sensitive insights within the data is essential for defining "quality". The extent of these damage-sensitive attributes directly influences the precision and effectiveness of any data-driven algorithm. Interestingly, compact datasets with rich features may outperform extensive datasets containing sparse, damage-sensitive details. Therefore, feature compression has frequently been employed as a strategy to address this issue.

1.3. Data-enrichment for CNN

CNN architecture is conventionally structured to process raw image (2D/3D) data and extract damage-sensitive features or patterns autonomously. Given its architecture's impartial nature, it is evident that these features usually take on numerical attributes, potentially limiting the incorporation of additional physics-based insights by researchers. As a consequence, the network may necessitate extensive datasets to derive a sufficient volume of numerical features. However, the extraction of features, particularly when they possess explicit numerical characteristics, through trial and error might yield sub-optimal predictive outcomes and can extend the duration and intensity of the training process.

As an alternative, researchers have exercised the liberty to employ certain techniques for extracting damage-sensitive features directly from the data before putting them into a CNN-based classification framework (Tang et al., 2020; Yao and Pakzad, 2012). This approach offers numerous advantages, including data compression and the creation of feature-rich representations. By reducing the data length, the computational load on the CNN-based network can be considerably reduced, leading to enhanced efficiency and estimation promptness. Furthermore, this preprocessing step aids in mitigating the influence of noise and outliers, thereby enhancing the precision and dependability of outcomes.

1.4. Auto-regressor for data compression and enrichment

Auto-regressive models have been identified as one such approach that can lead to the extraction of damage-intense features from the raw response data (Kosorus et al., 2012; Nair et al., 2006) especially when the enforced assumption on data normality suits the reality, FOWT dynamics being one such case. Kosorus et al. (2012) identified the coefficients of AR models as a suitable DSF that shows significant sensitivity to the introduction of practical levels of damage. In this context, the literature detailing AR-based approaches for anomaly detection is briefly discussed to substantiate the incorporation of AR-derived features in the current algorithm. For example, Nair et al. (2006) exploited initial three-order AR model coefficients as DSFs, and a subsequent t-test extracted the damage features. Kiremidjian et al. (2011) employed Gaussian mixture models for AR coefficients (ARCs) and further damage attributes were identified

based on the number of models used. Integration of AR coefficients as DSFs in a data-centric damage estimation setting has also been undertaken through both unsupervised and supervised approaches (Yao and Pakzad, 2012; Roy and Das, 2015; Cross et al., 2013).

1.5. The proposed approach

Leveraging CNN's classification efficiency without being burdened with rigorous feature engineering can, in turn, be helpful. Moreover, CNNs can adapt to varying noise levels and data variability, heightening the model's robustness and generalization capacity. This study, therefore, proposes data compression via AR modeling and subsequent extraction of DSFs from AR coefficients using CNNs. CNNs, with their capacity for hierarchical feature learning, can autonomously detect significant patterns within ARCs, thus negating the need for meticulous feature selection. This innovative amalgamation of CNNs into the damage identification process holds the potential not only to accelerate analyses but also to enhance prediction accuracy by enabling the model to directly learn crucial features from raw ARCs.

In this study, the combined use of ARCs and CNN models is explored for structural damage classification. ARCs offer interpretability by capturing temporal dependencies efficiently, reflecting the historical success of AR modeling in time series analysis. However, ARCs alone exhibit limitations, including the neglect of spatial information critical for structural damage classification and the potential oversight of changes in spatial distribution associated with damage. Additionally, AR models may struggle to capture the complex nonlinear behaviors inherent in structural damage. To address these limitations, the integration of CNN with ARC is proposed. CNNs excel in capturing spatial patterns, handling nonlinear relationships, and facilitating end-to-end learning from raw sensor data. This combined approach enhances damage classification accuracy by leveraging both temporal and spatial information, providing robustness to noise and sensor variability. The flexibility of CNN architectures further allows adaptation to various damage scenarios and sensor configurations, presenting a comprehensive and effective solution for SHM.

Further, this study explores the potential of such a coupled approach for an intricate structure type, i.e., FOWT. Given the limited comprehension of the physics underlying FOWT, particularly for its mooring network, this study aims to develop an algorithm for monitoring the condition of the mooring lines. While the primary focus is on creating an algorithm applicable to actual data collected from operational FOWTs, there is not much data available pertinent to the condition assessment of mooring lines sampled from real FOWT platforms, especially for both health and damaged conditions. Eventually, establishing the algorithm's reliability and effectiveness necessitates utilizing a replicative model as a control to simulate the required response datasets. This has been undertaken in this study via adopting NREL's OpenFast simulation package, tailor-made for offshore wind turbine simulations. The proposed methodology is further employed with the synthetic response to establish its efficacy and practicality. The developed approach is elaborated upon in the subsequent sections before demonstrating its efficacy through a series of numerical case studies.

2. Methodology

The overall approach is defined as a sequential step involving data compression and categorization. As mentioned, the data compression will be approached via AR modeling, ultimately defining the system dynamics with ARCs with considerably reduced dimensions compared to the original raw, noisy signal. Further, the capacity of CNN to classify non-distinguishable inputs will be investigated in its two-dimensional setup. Accordingly, both of these approaches necessitate comprehensive discussion, which will be elaborated upon in the subsequent sections. The overview of the proposed approaches is shown in Figure 1.

2.1. AR modelling

In ambient vibration conditions, the typical observation of structural response can be manifested as a series of random variables. According to Tang et al. (2020), employing an AR model is a viable strategy for representing such a process, provided that the sequence adheres to the conditions of normality and stationarity. Before modeling a sequence with the AR approach, it is recommended to eliminate any trend and then implement normalization. This dual step helps mitigate the negative impact of the amplitude and influences of external agents during sampling, ensuring a consistent mean and variance/covariance. This procedure can be executed in the following manner:

$$\mathbf{x}(t) = \frac{\tilde{\mathbf{x}}(t) - \mu}{\sigma} \tag{1}$$
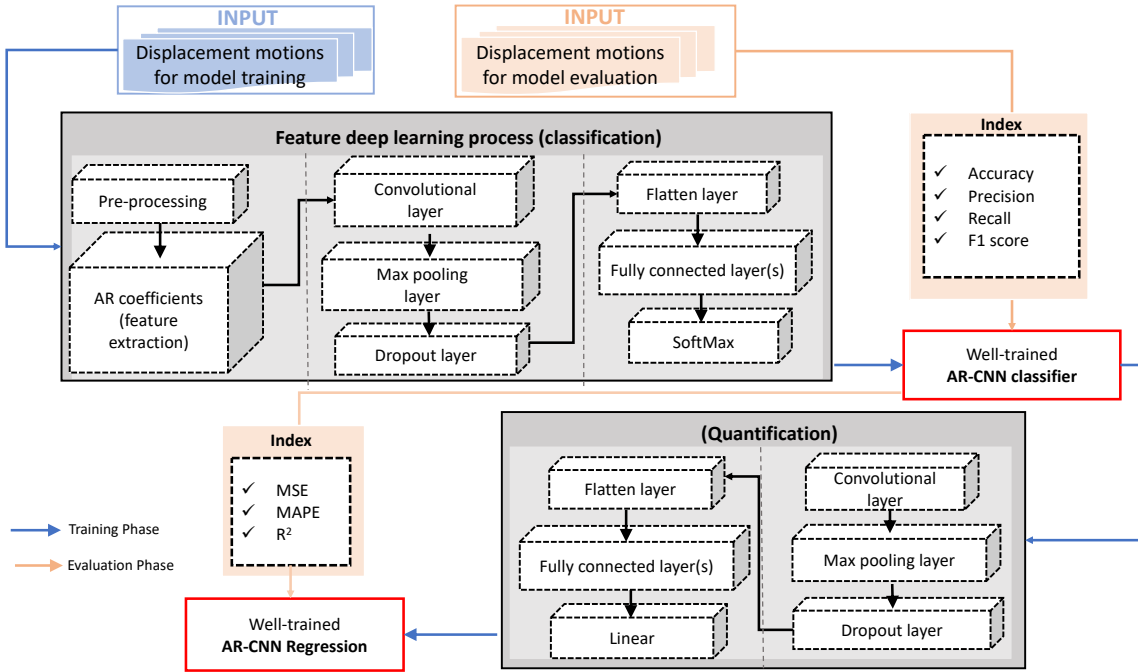
Figure 1: Flowchart illustrating the step-by-step methodology of the proposed approach.

with, μ and σ denoting the sample mean and sample standard deviations of the raw signal $\tilde{\mathbf{x}}(t)$, while $\mathbf{x}(t)$ is the normalized data. For an autoregressive moving-average (ARMA) (p, q) modeling of an arbitrary order p and MA order, q can be represented as a weighted sum of the last p values from previous time points, q weighted past noise terms, along with the current noise term e_t as:

$$\mathbf{x}(t) = \sum_{i=1}^{p} \phi_i \mathbf{x}_{t-i} + \sum_{i=1}^{q} \theta_i \mathbf{x}_{t-i} + e_t \tag{2}$$

where, ARCs $\{\phi_i\}, i = \{1, 2, \cdots, p\}$ and the MA coefficients (MACs) $\{\theta_i\}, i = \{1, 2, \cdots, q\}$ are the parameters of the model and e_t is the white noise that needs to be estimated. Following, three processes are typically involved in AR modeling i.e. establishing the model's hierarchy, estimating its parameters, and subsequently assessing the model's applicability while ensuring its computational efficacy and avoiding overfitting.

AR models have been widely studied as parametric representations for Structural Damage Detection (SDD). While ARMA models have also been used for SDD, AR's inherent invertibility property allows for the use of pure AR models to describe stochastic processes, as shown by Box et al. (2015). Despite their higher complexity, pure AR models have gained popularity due to their easier identification and estimation processes (Hoell and Omenzetter, 2016; Zheng and Mita, 2009). A study by Nair et al. (2006) explored the theoretical correlation between structural stiffness and ARCs, highlighting the utility of auto-regressive model coefficients (ARMCs) from ARMA models for detecting structural changes. This evidence underscores the superiority of AR coefficients, making them ideal for this study.

It is essential to emphasize that pure AR models constitute a subset of ARMA models with q set to 0. For an AR process of order p (AR(p)), a suitable value for p can be determined by identifying the lag at which the corresponding Partial Auto-Correlation (PAC) value becomes negligible. Similarly, the estimation of an appropriate order for the Moving Average (MA) component involves examining decreases in the Auto-Correlation Functions (ACFs) of the time series. A more systematic approach includes utilizing metrics such as the Akaike Information Criterion (AIC) and statistics related to identified prediction errors. This systematic approach helps define the dependence of each entry in the sequence on its predecessors. Consequently, the model order is chosen until the ACF reaches a significant level. To achieve this, the sample ACF r_j is typically calculated for a lag of j, as follows:

$$r_j = \frac{\sum_{t=j+1}^{n} \mathbf{x}(t)\mathbf{x}(t-j)}{\sum_{t=1}^{n} \mathbf{x}(t)^2}, j = 1, 2, \cdots \tag{3}$$

Using these ACFS, the PACFs, $(\hat{\varphi}_{j,k})$ are estimated as,

$$\hat{\varphi}_{jj} = \frac{r_j - \sum_{k=1}^{j-1} \hat{\varphi}_{j-1,k} r_{j-k}}{1 - \sum_{k=1}^{j-1} \hat{\varphi}_{j-1,k} r_k} \tag{4}$$

with,

$$\hat{\varphi}_{j,k} = \hat{\varphi}_{j-1,k} - \hat{\varphi}_{jj}\hat{\varphi}_{j-1,k-1}, k = 1, 2, \cdots, j-1 \tag{5}$$

In summary, this procedure aids in developing a broad comprehension of the suitable order range for the ARMA model, specifically when φ_j is likely to match $\hat{\varphi}_{jj}$. Subsequently, Eq.(5) is applied to determine the coefficients of the ARMA model across different orders. To adopt a more organized methodology, it is beneficial to incorporate metrics such as the AIC and to analyze statistics concerning the identified prediction errors. Calculating the residual e_t for the time series entails the following computation:

$$\hat{e}_t = \mathbf{x}(t) - \left\{ \sum_{i=1}^{p} \hat{\phi}_i \mathbf{x}_{t-i} + \sum_{i=1}^{q} \hat{\theta}_i \mathbf{x}_{t-i} \right\} \tag{6}$$

where $\hat{}$ denotes the estimated quantity.

Eventually, this procedure can be repeated for various model orders. Finally, the optimum model order p and q can be suitably chosen taking the basis of the AIC index, detailed in the following,

$$AIC(p) = \ln\left(\hat{\sigma}_e^2\right) + 2(p + q + 1)/s \tag{7}$$

with s being the size of the time series data and $\hat{\sigma}_e^2$ is the estimation of the noise variance. The initial term quantifies the model's likelihood, while the subsequent term serves as a regularisation factor for the combined complexity of the model with order $(p + q)$. If the derived model is accurate, the residuals exhibit characteristics resembling those of a Stationary White Gaussian Noise (SWGN) sequence. Consequently, one can assess the normality of the residuals by employing normal probability plots. Additionally, scrutiny of the residual ACF is possible. The unbiased j^{th} coefficient of the residual ACF can be computed as follows:

$$r_e[j] = \frac{1}{s-j} \sum_{i=1}^{s-j} e[i]e[i+j] \tag{8}$$

Eventually, the accuracy in the estimated model is supposed to ensure conformity of the residual to SWGN. Among the several available methods for analyzing the residual's normality, the quantile-quantile (Q-Q) map and ACF of residuals are used in the study. By characteristics, the Q-Q plot tends to be resembling a straight line for SWGN processes. Whereas the ACF of the residuals should come within 95% confidence bound to a suitable statistic (as mentioned in Brockwell and Davis (2002)).

To conduct this comprehensive test, the adapted Ljung-Box-Pierce statistic Q (originally introduced by Ljung and Box (1978)) is commonly employed. This statistic is defined as:

$$Q = n(n+2) \sum_{j=1}^{h} \hat{r}_e[j]/(n-j) \tag{9}$$

where $\hat{r}_e[j]$ is the estimated ACFs of residuals, h is the number of lags being tested for autocorrelation and n is the number of observations in the time series. The Q statistic is observed in the context of a SWGN process and in the case of a valid model, it aligns with a distribution χ^2 characterized by $j - p$ degrees of freedom as χ^2_{j-p}. This knowledge is employed for statistical hypotheses to test the estimated ARMA models.

2.2. Convolutional Neural Networks

In 1990, LeCun et al. (1990) introduced CNNs as powerful structures capable of automatically extracting intricate features from data. This architecture seamlessly combines feature extraction and classification, streamlining the learning process. Taking cues from the human visual cortex, CNNs were originally devised for 2D and 3D data like images and videos, primarily targeting visual recognition tasks. However, their utility has expanded significantly to encompass diverse domains such as speech recognition (Abdel-Hamid et al., 2012), natural language processing (Kim, 2014), classification of electrocardiogram (ECG) beats, power engine fault detection (Ince et al., 2016) and structural damage detection (Abdeljaber et al., 2018; Avci et al., 2017; Sharma and Sen, 2020), for example.
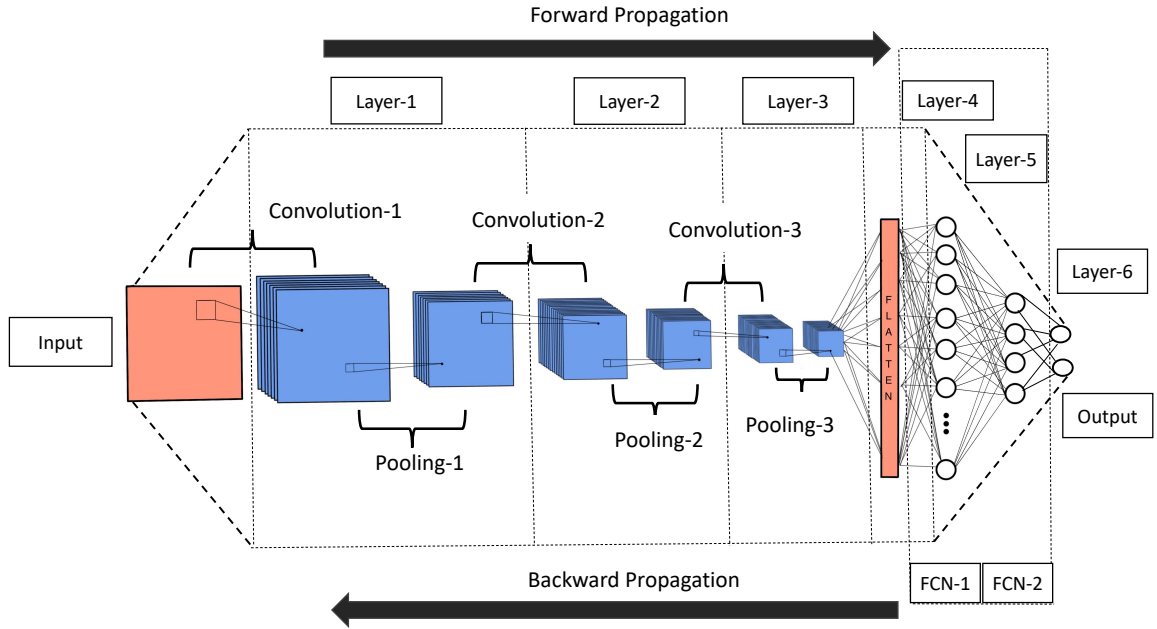
Figure 2: Schematic representation of the 2D-CNN network with three convolutional layers and two fully connected layers for multi-classification problem.

A typical vanilla CNN framework consists of convolutional, sub-sampling (pooling), and fully connected layers collectively termed classification layers. CNNs excel at processing grid-like data, making them effective for tasks involving spatial sequences (1D-CNNs) or images (2D-CNNs). Two key concepts distinguishing CNNs from Fully Connected Neural Networks (FCNs) are sparse connections and parameter sharing as highlighted by (Goodfellow et al., 2016). Input signals convolve with filters in the convolutional layer to identify pattern similarities. Sub-sampling layers use pooling to enhance feature maps, with multiple layers enriching them further. The classifier in the final layer associates inputs with labels. For 2D signals, convolution is expressed using eq.(10).

$$S(m, n) = I * K = \sum_i \sum_j I(i, j) K(m - i, n - j) \tag{10}$$

Here, $S(m, n)$ represents the resulting feature map, $I(i, j)$ denotes the input image, and $K(m - i, n - j)$ is the convolution kernel. When dealing with a 1D signal with an input as x_l^i, like a time series, the outcome of a 1D-CNN is given by eq.(11):

$$y_l^i = f\left(b_l^i + \sum_{j=1}^{N_{l-1}} Conv1D(w_{l-1}^{ji}, s_{l-1}^j)\right) \tag{11}$$

y_l^i represents the output, b_l^i denotes the bias of the ith neuron at layer l, s_{l-1}^j corresponds to the output of the ith neuron and w_{l-1}^{ji} symbolizes the kernel weight connecting the jth neuron from layer $l-1$ to the ith neuron at layer l. The function $'f()'$ signifies an activation function, such as ReLU, sigmoid, or tanh. The training procedure's primary goal is to identify the optimal set of kernels and biases that minimize the loss function. The distinction between 1D-CNN and 2D-CNN lies in their input, kernel, and feature map nature, which are either 1D or 2D.

Both 1D-CNN and 2D-CNN are instrumental in capturing essential features from these signals and learning intricate relationships within the data. Their ability to discern patterns and spatial correlations empowers them to uncover significant information in the input. This capability extends to learning inverse relationships, thereby enhancing their utility in tasks where understanding the interplay between different aspects of the data is crucial.

In CNNs, the Rectified Linear Unit (ReLU) activation function holds prominence. It is mathematically expressed as:

$$f(x) = \max(\mathbf{0}, \mathbf{x}) \tag{12}$$

Furthermore, the softmax activation function plays a pivotal role in the output layer of CNNs designed for multi-class classification tasks. Its formulation is given by:

$$f(x_i) = \frac{e^{x_i}}{\sum_{j=1}^{K} e^{x_j}} \tag{13}$$

with K denoting the number of classes.

Filters are diminutive weight matrices pivotal for feature extraction from input images. In CNNs, these filters convolve with input images to produce feature maps. As the filter traverses the image, distinct feature maps emerge at different positions.

For multi-class classification endeavors, the cross-entropy loss function is a staple in CNNs. It gauges the disparity between predicted and true probabilities, mathematically defined as:

$$H(p, q) = -\sum_{i=1}^{n} p_i \log(q_i) \tag{14}$$

where, p represents the true probability distribution and q signifies the predicted probability distribution with n is the number of classes..

When it comes to weight updates during training, CNNs typically employ the Adam optimization algorithm. This adaptive learning rate approach computes personalized learning rates for each parameter. Its equations are as follows:

$$m_t = \beta_1 m_{t-1} + (1 - \beta_1)g_t \tag{15}$$

$$v_t = \beta_2 v_{t-1} + (1 - \beta_2)g_t^2 \tag{b}$$

$$\hat{m}_t = \frac{m_t}{1 - \beta_1^t} \tag{c}$$

$$\hat{v}_t = \frac{v_t}{1 - \beta_2^t} \tag{d}$$

$$w_t = w_{t-1} - \alpha \frac{\hat{m}_t}{\sqrt{\hat{v}_t} + \epsilon} \tag{e}$$

In these equations, g_t denotes the gradient at time t, while m_t and v_t are the first and second-moment estimates, $\hat{m}_t$ and $\hat{v}_t$ represent bias-corrected estimates, α denotes the learning rate, ϵ prevents division by zero, and β_1 and β_2 determine exponential decay rates for moment estimates. The typical representation of a full network is given in Figure 2.

3. Case study
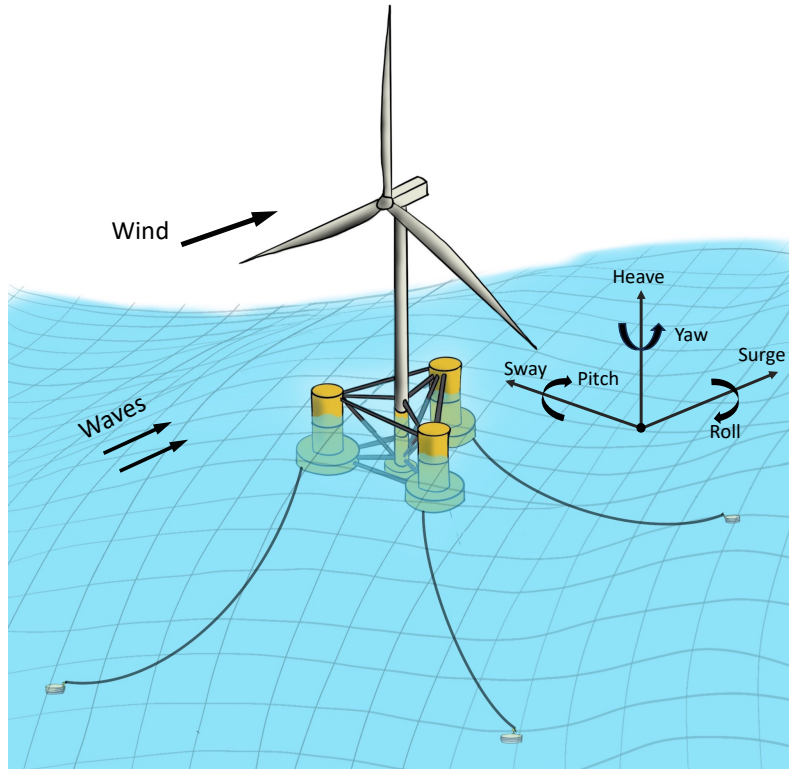
Figure 3: Schematic depiction of a semi-submersible Floating Offshore Wind Turbine (FOWT).

In the absence of actual data collected from real FOWTs, the open-source simulation tool OpenFast by the National Renewable Energy Laboratory (NREL) (Laboratory, 2021) can be employed to synthetically generate data representing both the damaged and healthy states of the FOWT. For validation purposes, the DeepcWind project has developed the benchmark OC4 5-MW semi-submersible FOWT within the OpenFast framework (Robertson et al., 2014), aiming to produce test data for relevant research applications. This approach aligns with common practices in wind turbine research, design, monitoring, and maintenance, as exemplified by previous studies (Gorostidi et al., 2023; Jonkman et al., 2018; Rinker et al., 2020; Jonkman et al., 2009). The simulated response serves as a valuable complement to the absence of real data, enabling the assessment of dynamic behavior under uncertain wind conditions and metocean conditions by replicating performance in a virtual environment.

In this study, the OC4 5-MW benchmark is treated as the actual structure for generating training and validation datasets. In order to represent the entire operational region of FOWT, the simulation incorporates a variety of metocean conditions and structural states within predetermined parameters that are not specific to any one site. These include wave height (H_s) spanning from 1 to 7 meters, peak period (T_p) varying between 8 to 15 seconds, wind speed (W_s) ranging from 1 to 10 m/s, and current ($Curr$) varying from 0.5 to 1.5 m/s, accounting for the randomness of the excitation. These metocean parameters are integrated into the simulation using established modules such as *InflowWind*, *HydroDyn*, and *Elastodyn* within OpenFAST.

Subsequently, the simulation generates single-point response time histories for all 6 degrees of freedom (*dof*s), covering both transverse and rotational motion of the FOWT platform, over a duration of 2000 seconds at a fixed sampling frequency of 40 Hz. The sampled response is then downsampled to 5 Hz, with the exclusion of the initial 500 seconds to avoid turbulence. The remaining downsampled signal serves as the input for the previously described monitoring network. Both displacement and acceleration are simulated in this process, and their relative sensitivity in detecting damage in the FOWT mooring system is later compared.

3.1. Replication of the degradation modes through simulation

Subsequently, it is crucial to pinpoint pertinent degradation modes for the creation of training input and corresponding labels. For any model-based SHM approach, selecting failure modes that induce changes in dynamic properties is imperative. In this investigation, three dominant mooring line degradation types are recognized: biofouling, corrosion damage, and bottom segment (anchorage) displacement.

Biofouling arises when diverse marine organisms, including seaweed, bacteria, plants, algae, and animals, accumulate on the mooring line. This accumulation adds weight and augments motion dampening. Harsh salty water and aerobic microbes on the line's surface contribute to pitting corrosion, reducing elasticity. Furthermore, inadequate friction between the anchor and the seabed may disrupt the bottom connection. This can prompt the entire FOWT system to shift towards a new equilibrium, potentially causing bottom section or anchorage displacement.

To recreate these degradation modes in a simulation, adjustments are applied to the OpenFAST module. Specifically, modifications are introduced within the MoorDyn module to emulate mooring damage effects. For example, to mimic biofouling's impact, MoorDyn's mass per unit length, typically 113.35 kg/m, is increased by 1-10%. This mass increment simulates notable biofouling on the mooring line. Pitting corrosion, which generally reduces stiffness and elasticity, is simulated by decreasing the mooring line's elasticity by 1-10%. Similarly, anchorage failure is replicated by shifting the bottom node of the mooring by a distance ranging from ±1 to ±10m in the simulation model, deviating from its initial position.

By incorporating these adjustments into the simulation, the OpenFAST model can replicate the various degradation modes encountered by mooring lines in real settings with sufficient accuracy. Subsequently, the model undergoes simulations under diverse metocean conditions in both intact and damaged states. A dataset comprising 20,000 scenarios is generated, encompassing 5000 sample cases for each of the four health states, totaling 5000×4 cases. Each case entails single-point response measurements across three *dof*s, acquired at a consistent 40 Hz sampling frequency over 2000 seconds. Stabilized responses are then resampled at 5 Hz, focusing on the interval from 500 to 2000 seconds for subsequent training and validation.

The training and validation database is subsequently structured using AR models. Following the earlier-detailed method in this manuscript, a suitable model order is chosen for this modeling approach. The ARCs corresponding to each sample database are further linked with specific damage cases (as labels) as previously outlined. These derived ARCs are subsequently trained against their respective labels using various classification methodologies. The AR coefficients work on the time domain data and can easily distinguish between any discrepancy in the motions.

3.2. Sensitivity assessment of the data

In the analysis of structural vibrations, time domain analysis, as opposed to frequency or spatial domain analyses, involves studying vibration signals in their original form, offering a high-dimensional representation of system dynamics. However, a drawback of time domain analysis is its vulnerability to measurement noise. Although the temporal representation facilitates addressing nonlinearity (damage-induced) or consequent time variance, not all signals effectively capture desired DSFs since various sensors may not be equally affected by such features. Therefore, it is crucial to assess the sensitivity of signals to monitored structural anomalies to ensure their suitability for analysis, as a model-based study consistently proves to be beneficial.

Evaluating sensitivity using signal power is a vital aspect of sensitivity assessment. This approach aids in quantifying the signal's strength or intensity, which can subsequently be linked to the magnitude of structural anomalies. Furthermore, tracking changes in signal power highlights shifts in the structure's dynamic behavior. Mathematically, for a continuous-time signal $x(t)$, the signal power S_p is defined as follows:

$$S_p = \lim_{T \to \infty} \int_{-T}^{T} x(t)^2 dt \tag{16}$$

In order to correlate the signal power with damage severity, the change in power (i.e. ΔS_j^k) is calculated for different damage cases as per the following equation:

$$\Delta S_j^k = 100 \frac{S_j^k - S_{av}^k}{S_{av}^k} \% \tag{17}$$

In this context, the metric ΔS_j^k represents the proportional power change (from S_{av}^k to S_j^k) in the kth signal caused by the jth damage scenario. The precision of this measure signifies the magnitude of damage—ideally, ΔS_j^k should exhibit higher values when $j = k$ and lower values otherwise.
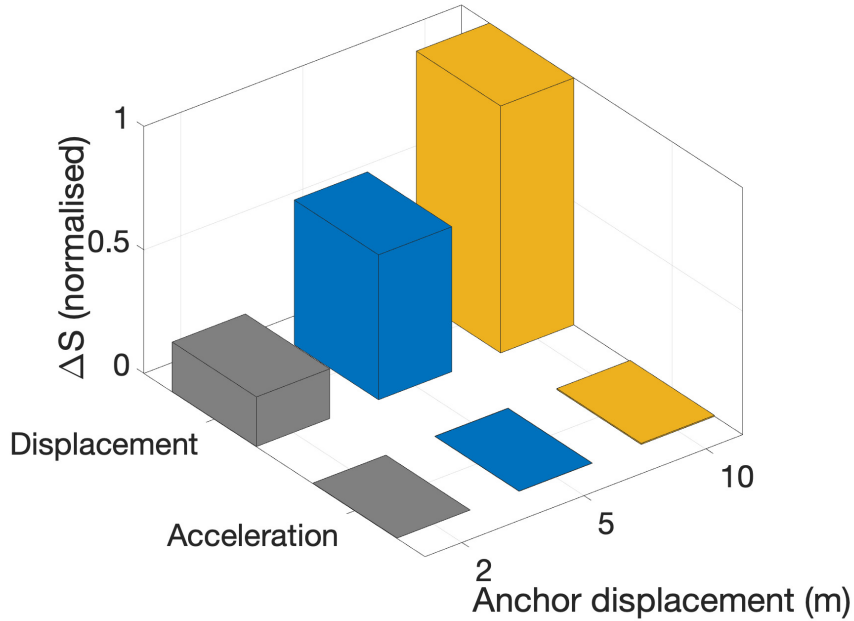
Figure 4: Sensitivity analysis for displacement and acceleration time history responses.

In this study, sensitivity assessment is conducted in a scenario involving the FOWT anchorage (displacement) for both acceleration and displacement signals and further compared in Figure4. Acceleration shows a direct link to external forces (F), reflecting the kinetic energy released by the structure. In contrast, displacement is more responsive to structural damage due to its relationship with stiffness and shape function.

Figure 5 depicts frequency responses for displacement and acceleration in both healthy and anchor displacement conditions. Accelerations show increased sensitivity to high-frequency excitations or dynamic events, influenced by structural mass. Higher frequencies accentuate the significance of the mass term in the equation $F = m \times a$, making accelerations more responsive to rapid motions. In contrast, displacement, linked to stiffness and shape changes, proves particularly effective in addressing challenges in damage assessment.

In structural engineering and analysis, a detailed grasp of the sensitivity of displacement *dofs* to structural anomalies is crucial. These anomalies span a range of damages and deteriorations, introducing complexity to the analytical landscape. Adding to this complexity is the recognition that structural responses are not only influenced by changes in structural conditions but also by the dynamic interaction of metocean conditions, which encompass meteorological and oceanographic factors. To thoroughly explore the sensitivity of these *dofs* to structural damage, a key technique involves the careful evaluation of signal autocorrelation.

Autocorrelation is a fundamental mathematical technique employed to assess the resemblance between a signal and its delayed version, searching for the lag at which the signal pattern recurs. This aids in determining the dataset's effective window before redundancy arises. This concept is critical for understanding the inherent traits of the signals in question. Consistent autocorrelation indicates a stable or periodic nature of the signal's behaviour. It implies that the system's response remains relatively consistent over time.

Applying this principle to structural systems, vibrations within the structure could converge to a uniform pattern, resulting in a stable autocorrelation trend. The graph shown in Figure 6 illustrates autocorrelation values for six distinct *dofs*. A meticulous examination of the graph reveals that autocorrelation patterns for sway, roll, and yaw motions exhibit minimal alteration. This finding implies that these specific *dofs* display steady and consistent system behavior considering the unidirection excitation in the surge direction. Such periodic signals are in actual, very little to offer for
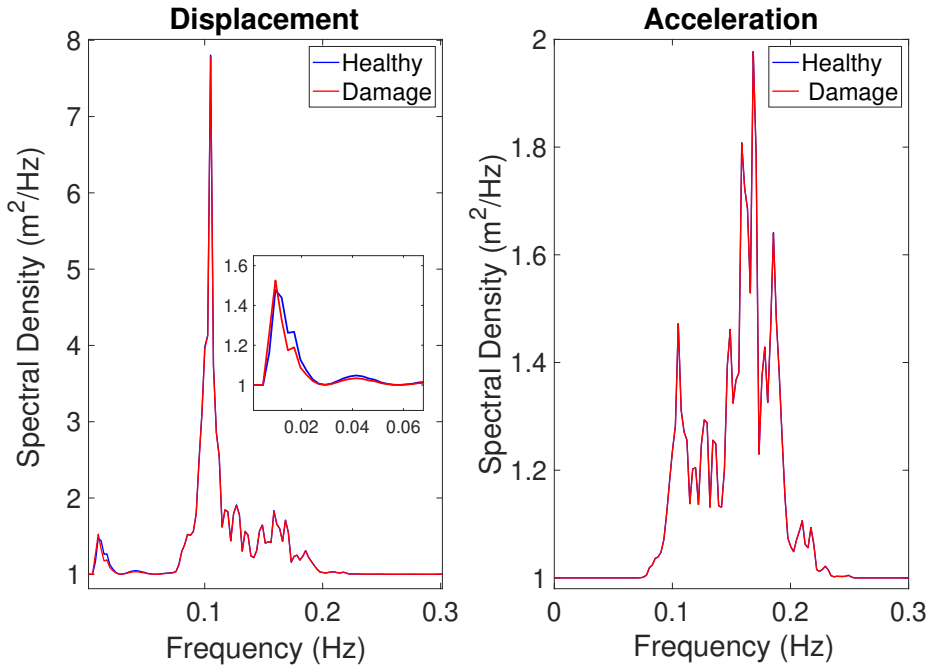
Figure 5: Comparison of frequency response for displacement and acceleration in surge motion.

system identification mainly due to the mechanical and geometrical symmetry of the system and therefore not taken into consideration for AR-CNN-based data analysis procedure.

In light of these findings, the subsequent focus of this study narrows down to three primary motions: surge, heave, and pitch. These are the *dofs* that demonstrate a more significant sensitivity to both structural anomalies and varying metocean conditions. By confining the investigation to these specific *dofs*, the study ensures a more detailed exploration of their behavior and sensitivity to external influences.

3.3. Extraction of ARCs

The initial phase of database construction involves formulating the AR models corresponding to all simulated responses and subsequently extracting the ARCs. A crucial step in this process is creating a reference AR or ARMA model based on the displacement time series of three *dofs* of the FOWT platform. An essential aspect of this procedure involves the preliminary determination of the model order since it is pivotal in discerning the inherent dynamics of the system. This primary model helps in determining the model order and also allows insight into the system dynamics. The AR models for all datasets are, however, crafted in the same order as the reference AR model for a healthy state. Maintaining a consistent model order establishes a solid foundation for comparative analysis and accurate evaluation.

Following these strategies, AR/ARMA models corresponding to various scenarios are systematically established. Initial separate evaluations of both AR and ARMA models are conducted, each undergoing comprehensive validation. Through a detailed analysis of ACF and PACF plots, the ARMA model, along with its corresponding AR coefficients, is employed in this study.

To determine the appropriate model order, the AIC values are computed for response samples of all three *dof*s across-model orders ranging from 1 to 50, considering q as 14. The average AIC value is presented in Figure 7. The AIC is observed to be stabilizing over increasing model order. Since with increasing model order, the computation increases exponentially, a practical value for the model order is typically identified from this graph using the elbow method.

For this study, the elbow could be found around the model order (16,14) and accordingly, ARMA(16,14) is selected for the optimal model order leaving scope for addressing unprecedented variability in the response. The chosen (16,14) model's validity is further confirmed through several statistical tests, including the Kolmogorov–Smirnov test and the modified Ljung–Box–Pierce statistic, which demonstrate its adherence to properties of zero-mean Gaussian white
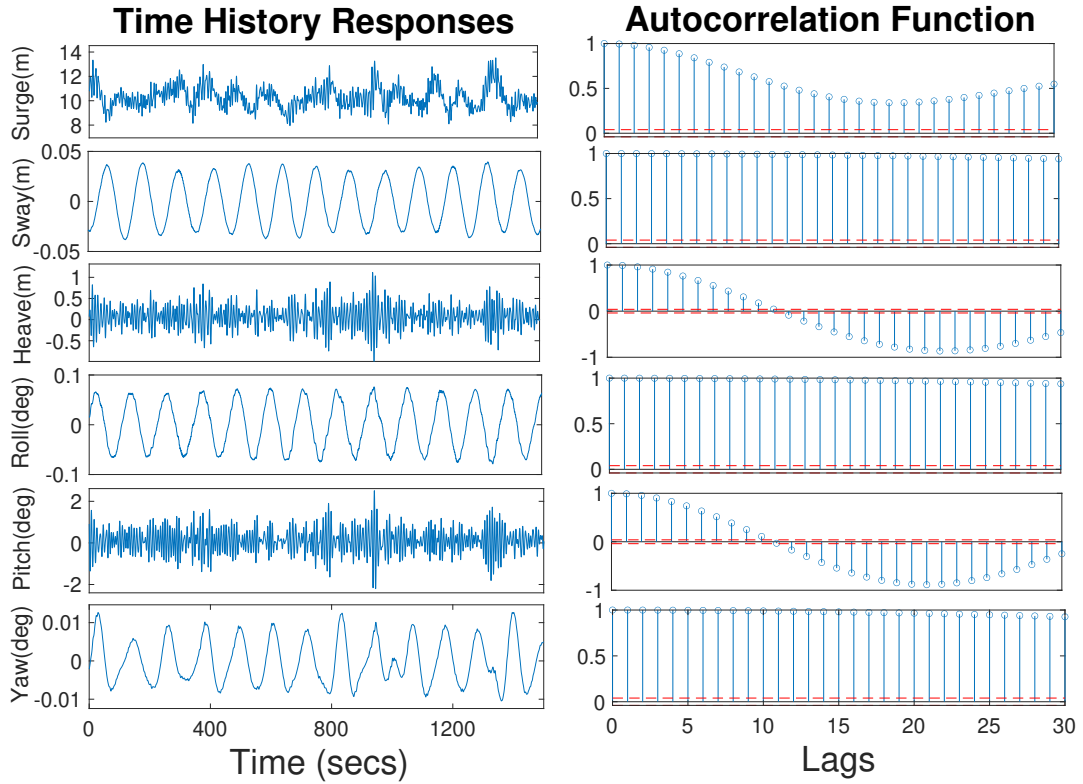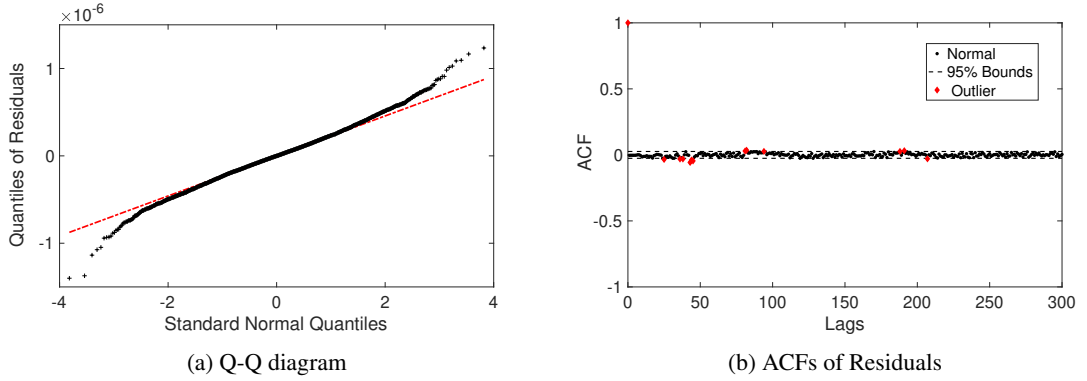
Figure 6: Auto-correlation plots demonstrating the relationship of different motions under a healthy operational state when $W_s=1$ m/s, $H_s=1$ m, $T_p=8$ s and $Curr=0.5$ m/s.
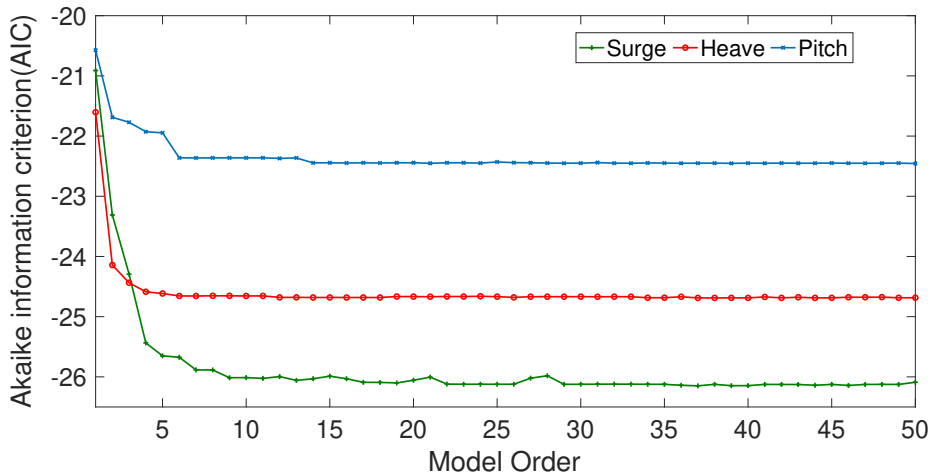
Figure 7: AIC evaluation for different orders of the AR Model considering all motions.

noise. Although the values deviate slightly from the reference straight line at extreme ends, they all consistently remain within the 95% confidence bounds(cf. Figure 8a). Additionally, the residual ACF is depicted in Figure 8b. Meanwhile, the modified Ljung-Box-Pierce statistic Q remains within the 95% confidence bounds even when examining the ACFs of the residual lags up to an order of 300. Notably, merely 13 values, accounting for 4.3% of the total, exceed the 95%

bound for a Gaussian white noise process. The results of these calculations consistently fell below the corresponding statistical thresholds set for the 95% confidence levels. Based on these tests and investigations, it can be concluded that the chosen ARMA(16,14) model is indeed valid.

(a) Q-Q diagram

(b) ACFs of Residuals

Figure 8: Normality test of residuals with Q-Q and auto-correlation of residuals.

To maintain brevity, the figure focuses on presenting results related to surge motion only, representing all other motions demonstrating similar behavior. Subsequently, the AR modeling approach is applied to model all other sample databases using the selected model order of (16,14). In this study, pure AR model coefficients are used, yielding 16×3 AR coefficient matrices for each database, without including a constant term. These coefficient matrices need to be classified based on their damage labels. To achieve this, a CNN is employed, treating the coefficient matrices as gray-scale images with a resolution of 16×3.
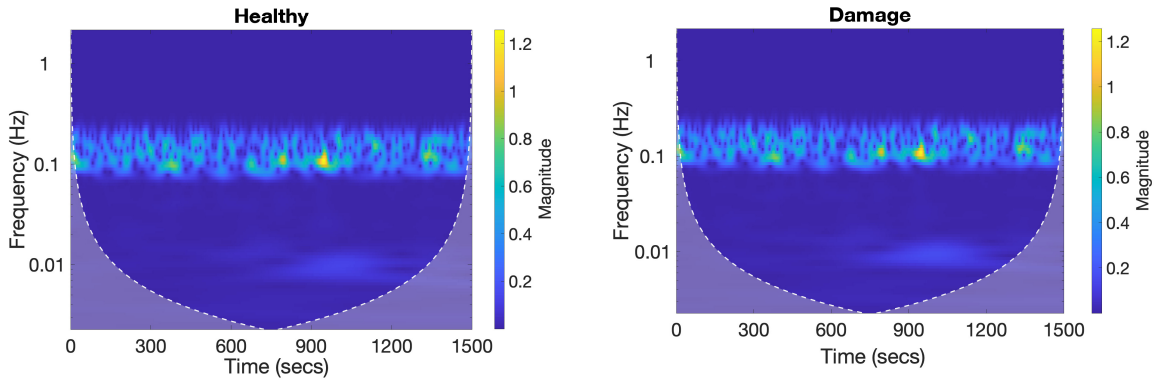
Figure 9: Time–Frequency analysis using Continuous Wavelet Transformation under healthy and damage state.

In delving deeper into the analysis, spectrograms are employed to shed light on potential challenges associated with the modal-domain formulation when applied to both damaged (anchor failure) and undamaged data. This visual representation facilitates the discernment of frequency content and variations within the dataset. Figure 9 illustrates that, however, no significant difference is observed between the damaged and undamaged data. The decision to employ AR coefficients is substantiated through spectrogram analysis, enabling data dimensionality reduction without a direct dependence on frequencies. This choice contrasts with frequency domain approaches, which also reduce data dimensionality but may overlook specific temporal dynamics.

Eventually, the employment of AR coefficients streamlines the extraction of relevant damage-related information in the temporal context, offering an alternative and potentially more insightful approach compared to conventional frequency-based methods. This strategy aims to overcome limitations inherent in modal-domain formulations when analyzing both damaged and undamaged data.

4. Damage detection and classification approach

Similar to typical data-based approaches, the consistent goal of standard network training has remained unchanged: striving for unbiased estimates while avoiding excessive over- or underfitting and ensuring broad prediction generalization across operational and structural scenarios. The selection of training and test datasets crucially involves two perspectives: firstly, achieving optimal training results necessitates a roughly equal distribution of samples across each category within the training set. Secondly, for meaningful comparative evaluations, the test set should encompass samples representing a spectrum of operational scenarios, including diverse metocean and health conditions.

The dataset for the current study is split in a stratified manner, with proportions of 80% for training and 20% for validation, resulting in 20000 training examples, and 4000 validation examples. This splitting ensures random shuffling whenever the algorithm is executed. Each training example is associated with a multi-class label as $\{0, 1, ., 4\}$, with 0 for healthy and the rest for the other four damage classes. Each input is a 16×3 matrix which is then sequentially reduced in dimension through stacks of convolution and pooling layers before being classified via a single fully connected layer. For the 2D-CNN framework, the key parameters include a learning rate of $1e-3$ with a batch size of 32. The multi-cross-entropy loss function is employed as the cost function. The training process utilizes the Adam optimization scheme, incorporating momentum and adaptive learning rate mechanisms. The training duration is 500 epochs, as shown in the loss curve depicted in Figure 10. Notably, during the prediction phase, exceptional performance is achieved with perfect accuracy, precision, and a recall value of 0.93. The network is trained on an Apple M1 Pro with an 8-core CPU, 16 GB of RAM, and a 14-core GPU. The code files are developed in a TensorFlow and Keras environment using the Python programming language. The computational time for training is 481.9 seconds.
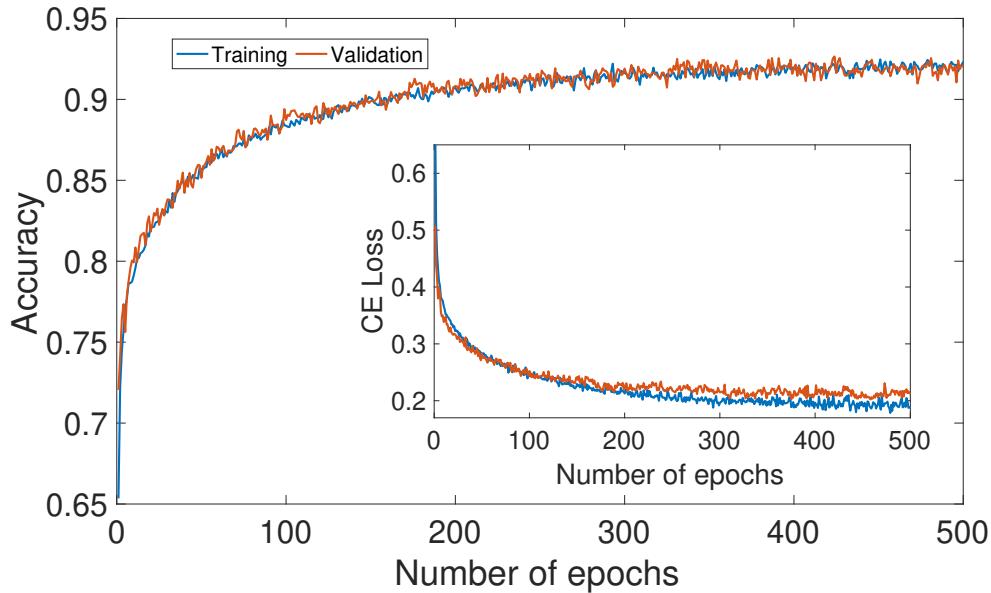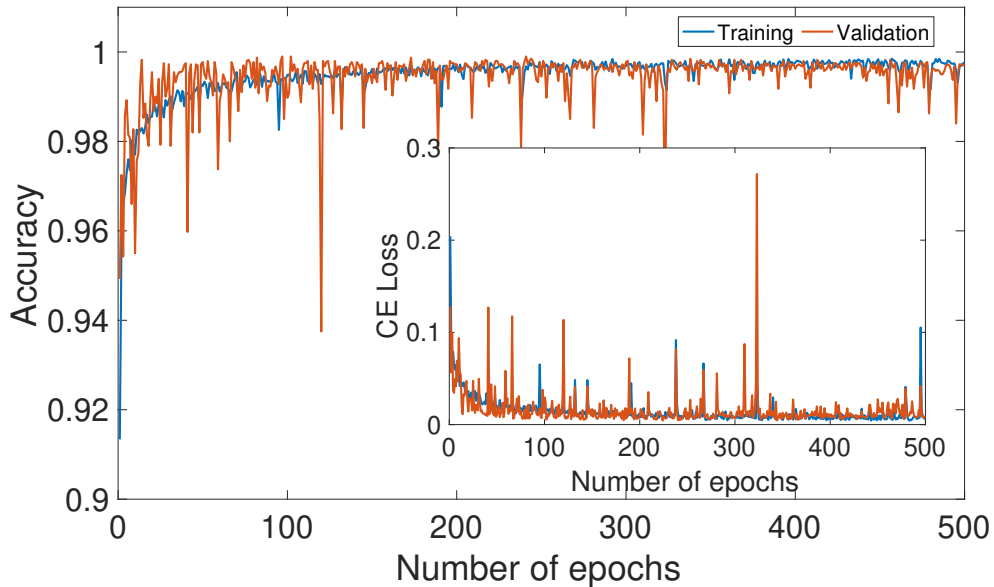

Figure 10: Accuracy and loss curves depicting the performance of the proposed AR-2DCNN network.

The architecture of 2D-CNN with AR is detailed in the following:

$$
\begin{aligned}
&\text{Conv2D(ReLU, 3x2, 16)} \rightarrow \text{Maxpooling } (2 \times 1) \\
&\text{Conv2D(ReLU, 2x2, 32)} \rightarrow \text{Maxpooling } (2 \times 1) \text{ Dropout(0.25)} \\
&\text{Conv2D(ReLU, 2x2, 64)} \rightarrow \text{Maxpooling } (2 \times 1) \text{ Dropout(0.25)} \\
&\text{Conv2D(ReLU, 2x2, 128)} \rightarrow \text{Maxpooling } (2 \times 1) \\
&\text{Flatten()} \\
&\text{Dense (ReLU, 100)} \rightarrow \text{Dropout(0.5)} \\
&\text{Dense (Softmax, 4)}
\end{aligned}
\tag{18}
$$

Next, the proposed approach is evaluated using the raw data, featuring sample sizes of 7501×3 each. A similar type of architecture is used on raw data for classification purposes. During the training of CNN on the raw data for this research, fluctuations in training loss, validation loss, and accuracy have been observed (cf.Figure 11). These fluctuations are inherent to the dynamic nature of the training process and can be influenced by various factors related to CNNs. The model's sensitivity to initial conditions, choices of hyper-parameters, and the characteristics of the training dataset can contribute to the observed variations. The oscillations in training loss indicate the adaptability of the model to the training data, while variations in validation loss reflect challenges in generalizing to unseen data. Simultaneously, fluctuations in accuracy underscore the evolving nature of the learning process, showcasing intermittent improvements and regressions. These fluctuations warrant thorough investigation to discern whether they arise from overfitting, underfitting, or other intricacies within the dataset. This network is trained using the online platform "Kaggle" with a GPU (T4 x 2) and its computational time is 4812.2 seconds.

Figure 11: Accuracy and loss curves obtained using 2D-CNN on raw data, illustrating the model's performance without preprocessing.

4.1. Predictions on wave seed randomness

In this study, an in-depth investigation is conducted into the influence of wave seed randomness on the accuracy of the proposed model trained for damage classification. The wave seed assumes a pivotal role in simulating the randomness of incident waves within the OpenFAST software, thereby introducing crucial variability into the environmental conditions. The AR-CNN model demonstrates promising outcomes during the training phase, achieving a commendable level of accuracy. Notably, diverse ranges of wave seeds are deliberately selected for training, facilitating a comprehensive understanding of the model's adaptability.

For testing, a distinct set of 60 samples is meticulously prepared for each damage class, incorporating diverse wave seeds. The proposed AR-CNN approach achieves a notable accuracy of approximately 85% during testing. In stark contrast, utilizing the raw CNN model with varying wave seed data results in a significant decline in classification accuracy, plummeting to merely 27% during testing while maintaining a high 99% during validation. This unexpected outcome highlights the heightened sensitivity of the model to fluctuations in wave seed randomness.

The findings emphasize the critical importance of accounting for the stochastic nature of environmental factors in both the training and testing phases of ML models for reliable damage classification in wind turbines. Consequently, the results affirm the superiority of the AR-CNN model when accounting for the randomness of the excitation.

The suitability of CNN as the classifier within the proposed AR-CNN framework is also compared against other conventional ML classifiers, specifically Support Vector Machines(SVM) (with kernels like Radial Bias Function
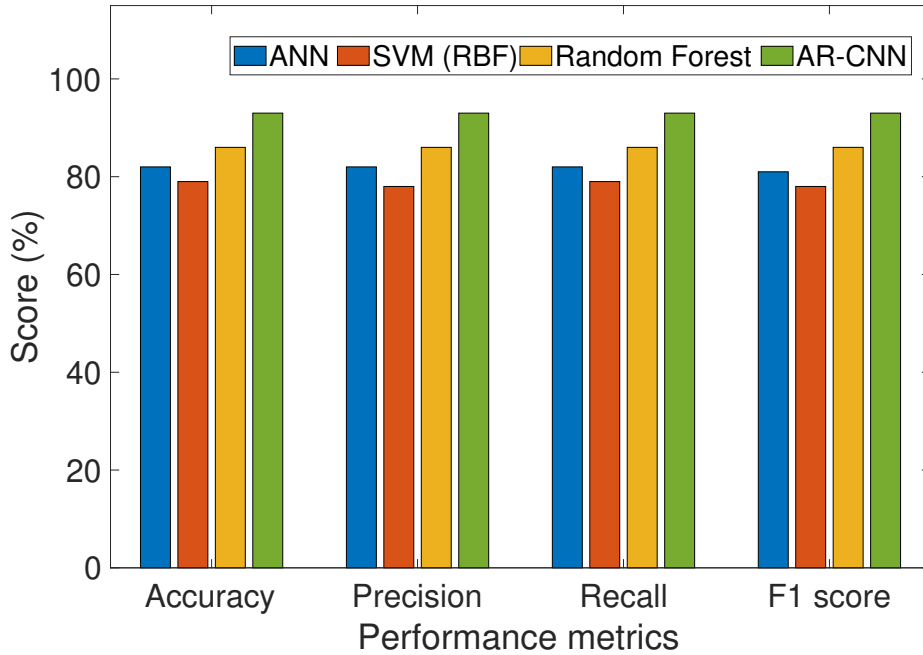
Figure 12: Performance metrics comparison of different classifiers, evaluating their effectiveness in classification tasks.

(RBF), Artificial Neural Networks (neurons = 2048) and Random Forest (trees = 30). To maintain consistency, the training and validation datasets utilized for MLP, random forest, and SVM are kept identical to those employed for CNN. As demonstrated in Figure 12, the CNN classifier attains the highest accuracy, reaching its best score of 93% for the validation dataset with random forest and ANN, securing second and third positions, respectively. This underlines the superior performance of CNN over other ML classifiers, which justifies its selection for the proposed framework.

This discrepancy in accuracy with other ML-based classifiers can, however, be attributed to the inherent non-linear relationship within the ARCs of the respective response across the three *dofs* considered, a characteristic effectively captured by the CNN architecture. CNN's ability to capture and retain these non-linear relationships proves pivotal in achieving and maintaining high levels of accuracy. To conduct a more comprehensive performance assessment, additional metrics such as precision, recall, and F1 score are introduced and compared. For the multi-classification task at hand, these metrics are calculated using micro-averaging, as depicted in Figure 12.

5. Damage quantification approach

The research extends the damage assessment methodology by introducing various specialized networks dedicated to assessing the quantification of damage within distinct classes, mentioned earlier. Identical network architectures are deployed for each damage class, utilizing the output from a prior damage classification step as input and damage severity (1-10%) as the target output.

Within the range considered for damage severity, it is further classified into three levels: mild (1-3%), moderate (4-7%), and severe (8-10%). Each neural network is trained on a dataset comprising 12, 000 samples, with each sample consisting of 1, 200 instances covering a severity range of 1%-10% . The dataset is split into training (80%), validation (10%) and testing (10%) sets to ensure model generalization. The training process employs Mean Square Loss as the cost function and utilizes the Adam optimization scheme for convergence. Model performance is assessed using metrics such as Mean Absolute Percentage Error (MAPE), Mean Absolute Error (MAE) and R^2. A 1D-CNN regression model is chosen for its effectiveness, configured with a learning rate of $1e - 3$ and a batch size of 32. The architecture of 1D-CNN for damage quantification is presented in the following.

Table 1
Performance metrics of damage cases for different severities

Cases	Severity	Recall	Precision	F1 Score
	Mild	0.980	0.852	0.911
Biofouling	**Moderate**	0.910	0.917	0.923
	Severe	0.923	0.997	0.9591
	Mild	0.992	0.807	0.890
Corrosion	**Moderate**	0.877	0.914	0.895
	Severe	0.91	1.00	0.956
	Mild	1.00	0.737	0.849
Anchor	**Moderate**	0.808	0.801	0.804
	Severe	0.785	0.989	0.8756

$$
\begin{aligned}
&\text{Conv1D(ReLU, 3x3, 64)} \rightarrow \text{Maxpooling } (2 \times 1) \\
&\text{Conv1D(ReLU, 3x3, 128)} \rightarrow \text{Maxpooling } (2 \times 1) \\
&\text{Flatten()} \\
&\text{Dense (ReLU, 512)} \rightarrow \text{Dropout(0.5)} \\
&\text{Dense (Linear, 1)}
\end{aligned} \tag{19}
$$
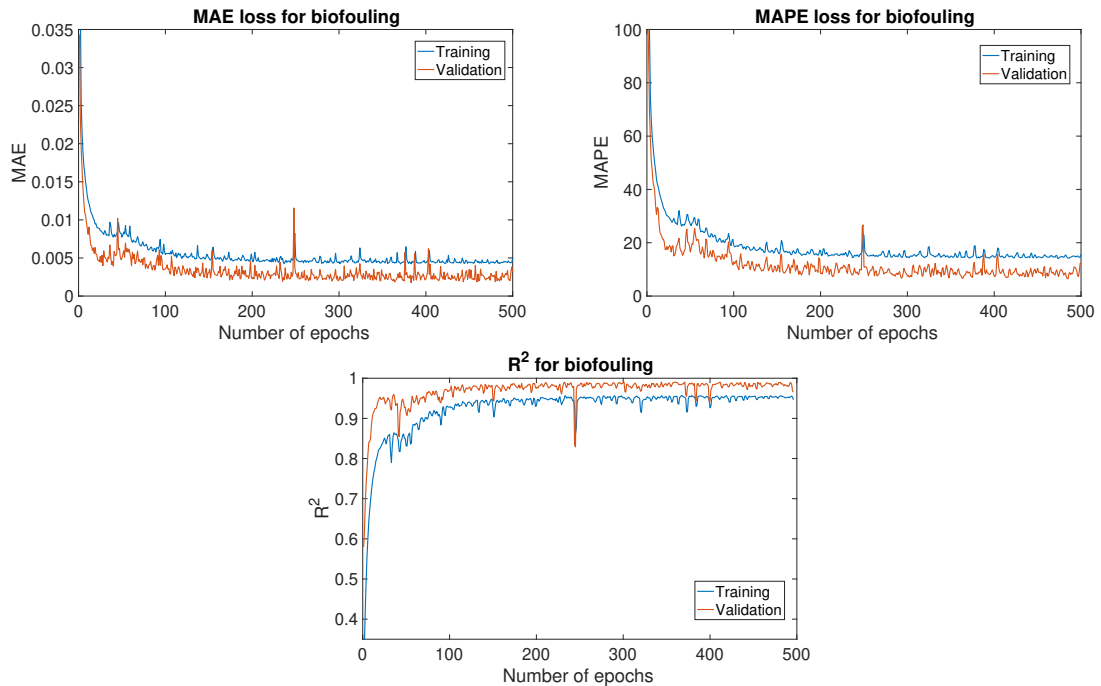
Figure 13: Mean Absolute Error (MAE), Mean Absolute Percentage Error (MAPE), and R-squared R^2 curves for damage quantification assessment.

The task of quantifying damage in mooring lines is addressed by training three distinct CNN regression networks, each dedicated to a specific damage class. Consistency in architecture across all classes is maintained to ensure standardized methodology and facilitate meaningful comparisons. To maintain conciseness, performance metrics during the training phase—MAPE, MAE and R^2—with a focus on biofouling cases are depicted in Figure13.

For a comprehensive evaluation, cross-plots and a confusion matrix, providing insights into the model's performance are presented in Figure14 only for biofouling scenarios for the sake of brevity while similar performance
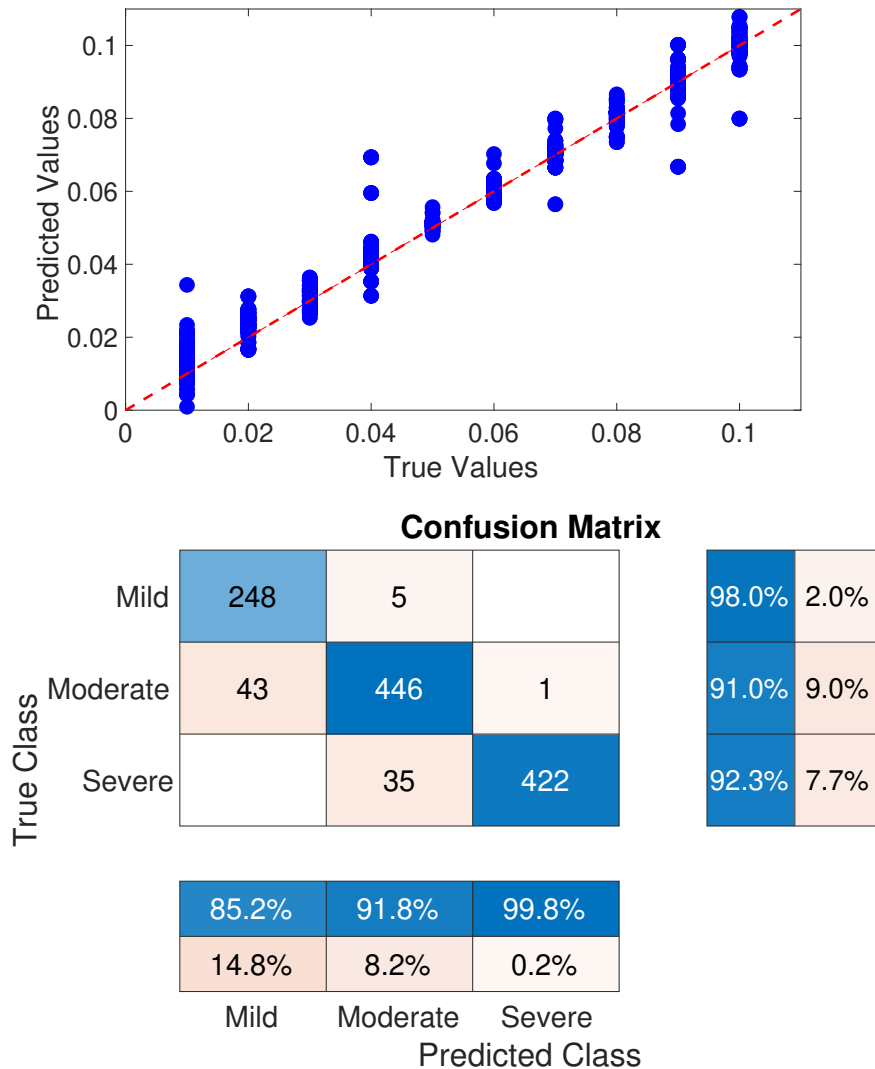
Figure 14: Cross-plots and confusion matrix analysis on the testing dataset for the biofouling case study.

is observed for other damage scenarios. For the damage cases of biofouling, corrosion, and anchor displacement, the corresponding MAPE and R^2 values are 11.333, 7.343, 7.049, and 0.974, 0.986, 0.989, respectively. This comparative analysis highlights the effectiveness of the model across different damage severity levels, displaying promising outcomes for all classes. Performance metrics for all damage severity classes, summarized in Table 1, reveal consistently positive results. Notably, even in cases of mild damage severity, commendable results are achieved with the proposed approach. This underscores the robustness of the method across the entire spectrum of damage severity levels.

The proposed method for quantifying damage is also compared to traditional ML-based classifiers, specifically SVM (RBF), Linear Regression, ANN (neurons = 2048) and Random Forest (trees = 30). To ensure fairness in the comparison, the datasets used for training, validation, and testing with competing alternatives are kept identical to those used for CNN regression. The MAPE and R^2 on the prediction test set are then compared with the DL-based CNN regression model, and the results are presented in Figure 15. The comparison reveals that the CNN regression model performs exceptionally well in the context of damage quantification.
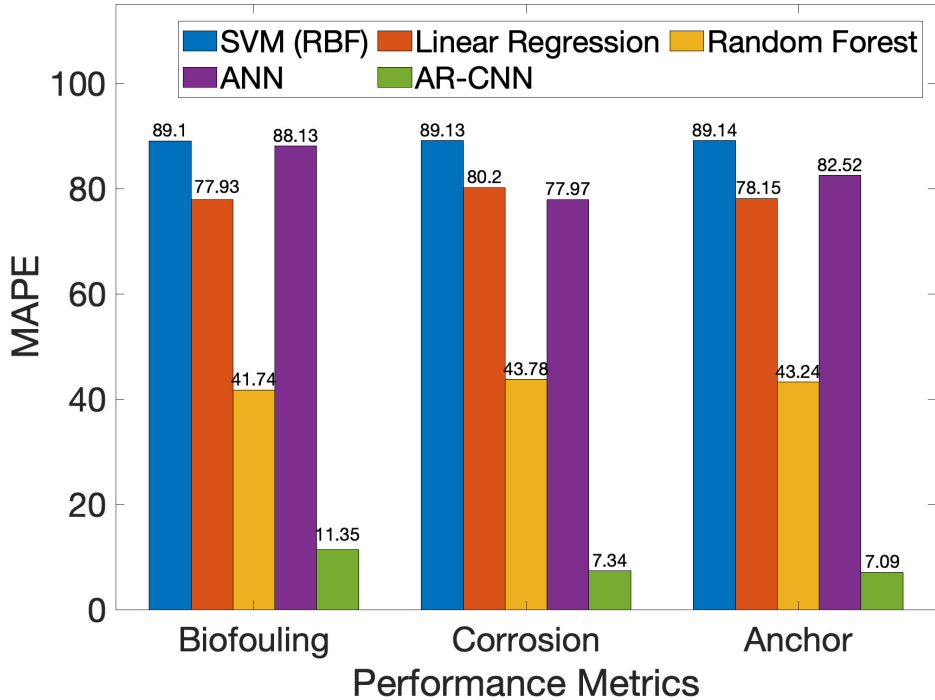
Figure 15: Comparative analysis of ML and AR-CNN (DL) models for damage quantification.

6. Conclusion

The study introduces an AR-CNN approach for damage identification in FOWT mooring, covering detection, classification, and quantification. In contrast to typical CNN-based methods that automatically extract numerical damage-sensitive features without leveraging the knowledge of system dynamics, the proposed approach exploits spatio-temporal correlation embedded in the sampled response by combining AR modeling with CNN. AR inculcates knowledge of system dynamics through a pseudo-physical framework of time series modeling, generating damage-sensitive sets of AR coefficients. The powerful classification capability of CNN further attributes these features to corresponding labels for damage classes and severity levels. The use of ARCs as damage sensitive features significantly compresses and enhances the quality of data fed to CNN for classification, leading to faster and more effective learning. When applied to mooring damage identification, even under uncertain forcing, the approach demonstrates substantially higher accuracy compared to typical other competing ML-based classifier networks, as evidenced by various quality indices. Ultimately, the research establishes the practicality of the proposed AR-CNN approach for real-time continuous monitoring, offering a more reliable network and promising cost reduction in Operation and Maintenance (O&M) expenses.

Subsequent to damage identification, further exploration of the network for damage prognosis, considering force history and structural properties, is recommended. Additionally, the adaptation of the proposed approach for various FOWT types with diverse damage scenarios under complex operational and extreme conditions, especially for simultaneous occurrences of multiple failure modes, can be envisioned.

7. Acknowledgements

8. Declaration of competing interest

There are no relevant financial or non-financial competing interests to report.

9. Data Availability Statement

Data and training code are available from the corresponding author upon reasonable request.

References

Abdel-Hamid, O., Mohamed, A.r., Jiang, H., Penn, G., 2012. Applying convolutional neural networks concepts to hybrid nn-hmm model for speech recognition, in: 2012 IEEE international conference on Acoustics, speech and signal processing (ICASSP), IEEE. pp. 4277–4280.

Abdeljaber, O., Avci, O., Kiranyaz, M.S., Boashash, B., Sodano, H., Inman, D.J., 2018. 1-d cnns for structural damage detection: verification on a structural health monitoring benchmark data. Neurocomputing 275, 1308–1317.

Atha, D.J., Jahanshahi, M.R., 2018. Evaluation of deep learning approaches based on convolutional neural networks for corrosion detection. Structural Health Monitoring 17, 1110–1128.

Augustyn, D., Tygesen, U.T., Ulriksen, M.D., Sørensen, J.D., 2019. Data-driven design and operation of offshore wind structures, in: The 29th International Ocean and Polar Engineering Conference, OnePetro.

Avci, O., Abdeljaber, O., Kiranyaz, S., Inman, D., 2017. Structural damage detection in real time: implementation of 1d convolutional neural networks for shm applications, in: Structural Health Monitoring & Damage Detection, Volume 7. Springer, pp. 49–54.

Bae, Y., Kim, M., Kim, H., 2017. Performance changes of a floating offshore wind turbine with broken mooring line. Renewable Energy 101, 364–375.

Banfield, S., Casey, N., Nataraja, R., 2005. Durability of polyester deepwater mooring rope, in: Offshore technology conference, OnePetro.

Benassai, G., Campanile, A., Piscopo, V., Scamardella, A., 2014. Ultimate and accidental limit state design for mooring systems of floating offshore wind turbines. Ocean Engineering 92, 64–74.

Box, G.E., Jenkins, G.M., Reinsel, G.C., Ljung, G.M., 2015. Time series analysis: forecasting and control. John Wiley & Sons.

Brindley, W., Comley, A.P., 2014. North sea mooring systems: how reliable are they?, in: International Conference on Offshore Mechanics and Arctic Engineering, American Society of Mechanical Engineers. p. V01AT01A025.

Brockwell, P.J., Davis, R.A., 2002. Introduction to time series and forecasting. Springer.

Cha, Y.J., Choi, W., Büyüköztürk, O., 2017. Deep learning-based crack damage detection using convolutional neural networks. Computer-Aided Civil and Infrastructure Engineering 32, 361–378.

Chen, F.C., Jahanshahi, M.R., 2017. Nb-cnn: Deep learning-based crack detection using convolutional neural network and naïve bayes data fusion. IEEE Transactions on Industrial Electronics 65, 4392–4400.

Coulling, A.J., Goupee, A.J., Robertson, A.N., Jonkman, J.M., Dagher, H.J., 2013. Validation of a fast semi-submersible floating wind turbine numerical model with deepcwind test data. Journal of Renewable and Sustainable Energy 5, 023116.

Cross, E., Worden, K., Farrar, C., 2013. Structural health monitoring for civil infrastructure, in: Health Assessment of Engineered Structures: Bridges, Buildings and Other Infrastructures. World Scientific, pp. 1–31.

Duan, F., Hu, Z., Niedzwecki, J., 2016. Model test investigation of a spar floating wind turbine. Marine Structures 49, 76–96.

Goodfellow, I., Bengio, Y., Courville, A., 2016. Deep learning. MIT press.

Gorostidi, N., Pardo, D., Nava, V., 2023. Diagnosis of the health status of mooring systems for floating offshore wind turbines using autoencoders. Ocean Engineering 287, 115862.

Hoell, S., Omenzetter, P., 2016. Optimal selection of autoregressive model coefficients for early damage detectability with an application to wind turbine blades. Mechanical Systems and Signal Processing 70, 557–577.

Huang, C.C., Pan, J.Y., 2010. Mooring line fatigue: A risk analysis for an spm cage system. Aquacultural engineering 42, 8–16.

Ince, T., Kiranyaz, S., Eren, L., Askar, M., Gabbouj, M., 2016. Real-time motor fault detection by 1-d convolutional neural networks. IEEE Transactions on Industrial Electronics 63, 7067–7075.

Jahangiri, V., Mirab, H., Fathi, R., Ettefagh, M.M., 2016. Tlp structural health monitoring based on vibration signal of energy harvesting system. Latin American Journal of Solids and Structures 13, 897–915.

Jamalkia, A., Ettefagh, M.M., Mojtahedi, A., 2016. Damage detection of tlp and spar floating wind turbine using dynamic response of the structure. Ocean Engineering 125, 191–202.

Jonkman, J., Butterfield, S., Musial, W., Scott, G., 2009. Definition of a 5-mw reference wind turbine for offshore system development URL: https://www.osti.gov/biblio/947422, doi:10.2172/947422.

Jonkman, J.M., Wright, A.D., Hayman, G.J., Robertson, A.N., 2018. Full-system linearization for floating offshore wind turbines in openfast, in: International Conference on Offshore Mechanics and Arctic Engineering, American Society of Mechanical Engineers. p. V001T01A028.

Kim, Y., 2014. Convolutional neural networks for sentence classification. arXiv preprint arXiv:1408.5882 .

Kiremidjian, A.S., Kiremidjian, G., Sarabandi, P., 2011. A wireless structural monitoring system with embedded damage algorithms and decision support system. Structure and Infrastructure Engineering 7, 881–894.

Kosorus, H., Höllrigl-Binder, M., Allmer, H., Küng, J., 2012. On the identification of frequencies and damping ratios for structural health monitoring using autoregressive models, in: 2012 23rd International Workshop on Database and Expert Systems Applications, IEEE. pp. 23–27.

Laboratory, N.R.E., 2021. Openfast documentation. URL: https://openfast.readthedocs.io/en/main/. (Online; Accessed 10 February 2022).

LeCun, Y., Boser, B.E., Denker, J.S., Henderson, D., Howard, R.E., Hubbard, W.E., Jackel, L.D., 1990. Handwritten digit recognition with a back-propagation network, in: Advances in neural information processing systems, pp. 396–404.

Li, Y., Le, C., Ding, H., Zhang, P., Zhang, J., 2019. Dynamic response for a submerged floating offshore wind turbine with different mooring configurations. Journal of Marine Science and Engineering 7, 115.

Liu, Y., Xiao, Q., Incecik, A., Peyrard, C., Wan, D., 2017. Establishing a fully coupled cfd analysis tool for floating offshore wind turbines. Renewable Energy 112, 280–301.

Ljung, G.M., Box, G.E., 1978. On a measure of lack of fit in time series models. Biometrika 65, 297–303.

Ma, K.t., Shu, H., Smedley, P., L'Hostis, D., Duggal, A., 2013. A historical review on integrity issues of permanent mooring systems, in: Offshore technology conference, OnePetro.

Mentes, A., Helvacioglu, I.H., 2011. An application of fuzzy fault tree analysis for spread mooring systems. Ocean Engineering 38, 285–294.

Modarres, C., Astorga, N., Droguett, E.L., Meruane, V., 2018. Convolutional neural networks for automated damage recognition and damage type identification. Structural Control and Health Monitoring 25, e2230.

Nair, K.K., Kiremidjian, A.S., Law, K.H., 2006. Time series-based damage detection and localization algorithm with application to the asce benchmark structure. Journal of Sound and Vibration 291, 349–368.

Rafiee, J., Arvani, F., Harifi, A., Sadeghi, M., 2007. Intelligent condition monitoring of a gearbox using artificial neural network. Mechanical systems and signal processing 21, 1746–1754.

Rinker, J., Gaertner, E., Zahle, F., Skrzypiński, W., Abbas, N., Bredmose, H., Barter, G., Dykes, K., 2020. Comparison of loads from hawc2 and openfast for the iea wind 15 mw reference wind turbine, in: Journal of Physics: Conference Series, IOP Publishing. p. 052052.

Robertson, A., Jonkman, J., Masciola, M., Song, H., Goupee, A., Coulling, A., Luan, C., 2014. Definition of the semisubmersible floating system for phase II of OC4. Technical Report. National Renewable Energy Lab.(NREL), Golden, CO (United States).

Roy, S., Das, T.K., 2015. Plant mediated green synthesis of silver nanoparticles-a. Int. J. Plant Biol. Res 3, 1044–1055.

Schlechtingen, M., Santos, I.F., 2011. Comparative analysis of neural network and regression based condition monitoring approaches for wind turbine fault detection. Mechanical systems and signal processing 25, 1849–1875.

Sharma, S., Sen, S., 2020. One-dimensional convolutional neural network-based damage detection in structural joints. Journal of Civil Structural Health Monitoring 10, 1057–1072.

Sharma, S., Sen, S., 2021. Bridge damage detection in presence of varying temperature using two-step neural network approach. Journal of Bridge Engineering 26, 04021027.

Sharma, S., Sen, S., 2023. Real-time structural damage assessment using lstm networks: regression and classification approaches. Neural Computing and Applications 35, 557–572.

Soukup, D., Huber-Mörk, R., 2014. Convolutional neural networks for steel surface defect detection from photometric stereo images, in: International Symposium on Visual Computing, Springer. pp. 668–677.

Tang, Q., Zhou, J., Xin, J., Zhao, S., Zhou, Y., 2020. Autoregressive model-based structural damage identification and localization using convolutional neural networks. KSCE Journal of Civil Engineering 24, 2173–2185.

Thies, P.R., Johanning, L., Harnois, V., Smith, H.C., Parish, D.N., 2014. Mooring line fatigue damage evaluation for floating marine energy converters: Field measurements and prediction. Renewable Energy 63, 133–144.

Tong, Z., Gao, J., Zhang, H., 2017. Recognition, location, measurement, and 3d reconstruction of concealed cracks using convolutional neural networks. Construction and Building Materials 146, 775–787.

Tygesen, U.T., Jepsen, M.S., Vestermark, J., Dollerup, N., Pedersen, A., 2018. The true digital twin concept for fatigue re-assessment of marine structures, in: International Conference on Offshore Mechanics and Arctic Engineering, American Society of Mechanical Engineers. p. V001T01A021.

WindEurope, 2021. Spain issues plan for up to 3 gw offshore wind by 2030 – in perfect time for windeurope 2022 in bilbao! (Accessed 18 July 2022).

WindEurope, 2022. Europe can expect to have 10 gw of floating wind by 2030. (Accessed 18 July 2022).

Xu, Y., Bao, Y., Chen, J., Zuo, W., Li, H., 2019. Surface fatigue crack identification in steel box girder of bridges by a deep fusion convolutional neural network based on consumer-grade camera images. Structural Health Monitoring 18, 653–674.

Yao, R., Pakzad, S.N., 2012. Autoregressive statistical pattern recognition algorithms for damage detection in civil structures. Mechanical Systems and Signal Processing 31, 355–368.

Zheng, H., Mita, A., 2009. Localized damage detection of structures subject to multiple ambient excitations using two distance measures for autoregressive models. Structural Health Monitoring 8, 207–222.